Electric field and temperature measurement using ultra wide bandwidth pigtailed electro-optic probes

Maxime Bernier, Gwenaël Gaborit, Lionel Duvillaret, Alain Paupert, J.L. Lasserre

Electric field and temperature measurement using ultra wide bandwidth pigtailed electro-optic probes

Maxime Bernier,[1] Gwenaël Gaborit,[2] Lionel Duvillaret[1,*], Alain Paupert[3] and Jean-Louis Lasserre[3]

[1]IMEP-LAHC, UMR CNRS 5130, Minatec-INPG, 3 parvis Louis Néel, BP 257, 38016 Grenoble Cedex 1, FRANCE

[2]IMEP-LAHC, UMR CNRS 5130, Université de Savoie, Campus Scientifique, 73376 Le Bourget du Lac Cedex, FRANCE

[3]DGA /D4S/MRIS/Centre d'Études de Gramat, 46500 Gramat, FRANCE

[*]Corresponding author: lionel.duvillaret@inpg.fr

We present pigtailed electro-optic probes that allow a simultaneous measurement of high frequency electric fields and temperature using a unique laser probe beam. This has been achieved by the development of a novel probe design associated with a fully automated servo-controlled optical bench, initially developed to stabilize the electric field sensor response. The developed electro-optic probes present a stable response in outdoors conditions over time duration exceeding 1 hour, a frequency bandwidth from kHz to tens of GHz with a sensitivity of 0.7 $V.m^{-1}.Hz^{-1/2}$ and a temperature accuracy of 40 mK.

OCIS codes: 280.0280, 280.3420, 260.1440, 280.6780.

Introduction

In the field of high power microwave (HPM) measurements, ultra wide band (UWB) antennae are usually used. However, due to their metallic structure, antennae are greatly invasive and can be used only in the far field region; they are also unable to cover more than 3 or 4 decades of frequency [1]. Moreover, the size of UWB antennae make them incompatible with measurements inside equipments of reduced size. The recent development of pigtailed electro-optic (EO) sensors [2] could constitute a competitive alternative to antennae as they can bring solutions to the above-mentioned drawbacks. However, EO probes that were developed up to now suffer from the drift of their response with the temperature. Indeed, since these probes are based on a change of the eigen refractive indices of an EO crystal with the applied E field, they are also sensitive to the temperature as the EO crystal eigen refractive indices also depend on the temperature. Different solutions have been proposed to solve this problem like using a specific orientation of the EO crystal that minimizes thermal effects [3]. None of these solutions are completely satisfactory as they require electrical bias [4], laser wavelength control [5], complex designs or with low tolerances [6] … to get rid of the temperature dependent sensor response. R. Claverie *et al.* [7] have recently exploited this drawback to make an EO-crystal based temperature sensor.

We present here a novel millimeter-size UWB pigtailed EO probe covering more than 7 decades of frequency (kHz-GHz frequency range) and allowing getting simultaneously one specific component of the HPM E field and the probe temperature. This EO probe is associated with a servo-controlled optical system that is continuously locked on an optimal working point. The EO probe temperature is then deduced from the values of the parameters that permit to the system to compensate thermal drifts.

The simultaneous measurement of the probe temperature could bring complementary information. For example, we could imagine determining the energy of a single shot HPM signal by measuring the temperature increase of an EO probe surrounded by a microwave and thus acting as a calorimeter [8].

In order to validate this new concept of optical probe, we have built a $LiTaO_3$ pigtailed EO probe which has been characterized. We have obtained a frequency bandwidth exceeding 10 GHz, an E-field sensitivity of ~ 0.7 $V.m^{-1}.Hz^{-1/2}$ and a temperature accuracy of ~ 40 mK.

The paper is divided into three sections. In the first section, we present the principle of the optical probe together with the whole optical bench. The second section is dedicated to the theory and the last one to the experimental validation.

Principle

EO measurement of E fields using the Pockels' effect [9] is commonly used since the eighties. At first, it was employed to probe guided E fields propagating in electronic circuits [10]. For now ten years, it has been extended to E field mapping [11]. Most of EO probes are based on polarization state modulation (PSM), i. e. on the modification of the polarization state of a laser probe beam during its propagation through an EO crystal. The PSM is due to the E-field induced birefringence of the crystal but depends also on the crystal intrinsic birefringence variations which are linked to its temperature change [12]. Consequently, if E-field and temperature induced birefringences take place on different time scales, it should be possible in principle to distinguish them. This is presently the case when measuring E fields at frequencies higher than 1 kHz as thermal variations occur at very low frequencies. Indeed, an EO crystal being irradiated by HPM presents a low pass filter thermal behavior which is governed by its RC time constant

where C represents is heat capacity and R the thermal resistor between the EO crystal and an ambient temperature thermostat.

The problem is getting more complicated when one deals with pigtailed probes. As the useful information is carried by the polarization state of the laser probe beam, a polarization maintaining fiber (PMF) must be used to carry a linearly polarized laser probe beam from the laser source to the EO crystal. Although the PMF ensures this condition via the alignment of the laser polarization with one of its neutral lines, the polarization state of the laser probe beam is no more linear on the way back after propagating through the EO crystal. In our experimental setup, we have used an 18-m long PMF between the EO probe and the optical bench. Consequently, the propagation trough the PMF will induce an uncontrolled phase difference between the two eigenpolarizations, this phase difference depending on the temperature of the PMF [13]. Thus, it seems impossible to dissociate a temperature change of the PMF from a temperature change of the EO crystal.

Before dealing with this problem, let us remind that we get a linear response of the E field measurement with a maximized sensitivity if we are able to convert the polarization state of the laser probe beam –coming out from the PMF after its propagation through the EO crystal of physical length L– into a linear polarization state and then to split it using a polarizing beam splitter into two balanced optical beams whose powers are measured [14]. These two optical powers write:

$$P_{\frac{1}{2}} = \frac{P_{inc}}{2}\left(1 \pm \phi_E\right) = \frac{P_{inc}}{2}\left(1 \pm \frac{2\pi\,\overrightarrow{\Delta K}\cdot\vec{E}\,L_{eff}}{\lambda}\right) \tag{1}$$

where P_{inc} is the optical power at wavelength λ impinging onto the polarizing beam splitter. ϕ_E is the E-field induced phase difference between the two eigenpolarizations in the EO crystal of effective length $L_{eff} = 2\,L$ and $\overrightarrow{\Delta K}$ is the sensitivity vector [15]. As seen in Eq. (1), the only E-field component that leads to a variation of the optical powers received by the photodetectors is the one which is parallel to the sensitivity vector $\overrightarrow{\Delta K}$, this latter one depending on the EO crystal and on the direction of the laser probe beam inside the EO crystal.

In order to get the required polarization state at the entrance of the polarizing beam splitter, two birefringent plates are required: a $\lambda/4$ plate Q1 is used to convert the undefined polarization state into a linear polarization state and a $\lambda/2$ plate H1 is used to balance the optical powers received by the two photodetectors which are represented in Fig. 1 as PD1 and PD2. As seen on the sketch of the whole optical bench included the pigtailed EO probe (see Fig. 1), another detection path has been added to guarantee that we get the required polarization state. Indeed, one would get also balanced photocurrents if the laser beam impinging onto the 1st Wollaston prism is circularly polarized. In order to eliminate the cases for which we get perfectly balanced optical powers received by PD1 and PD2 without having a linear polarization state at the entrance of the 1st Wollaston prism, a $\lambda/4$ plate Q2 has been added on a second detection path. The neutral lines of this $\lambda/4$ plate and the axes of the 2nd Wollaston prism make an angle of 0° and of 45° about the axes of the 1st Wollaston prism, respectively. With such a configuration, it is easy to show that optical powers received by PD1 and PD2 on one hand and by PD3 and PD4 on the other hand will be both perfectly balanced if and only if we have the right linear polarization state at the entrance of the 1st Wollaston prism: these two conditions define the optimal working point of the system.

Using Jones' matrices formalism [16], let us see in the next section why the insertion of a $\lambda/4$ plate between the PMF and the EO crystal, such as the neutral lines of a $\lambda/4$ plate make an angle of 45° about the ones of the PMF, leads to a dissociation of PMF temperature change from EO crystal temperature change [17].

Theory

The Jones' matrix of the EO probe, represented in Fig. 2, is:

$$M_{probe} = M_{\lambda/4} \cdot R_{-\alpha} \cdot \begin{pmatrix} \exp(-j\Delta\phi/2) & 0 \\ 0 & \exp(j\Delta\phi/2) \end{pmatrix} \cdot R_{\alpha} \cdot M_{\lambda/4} \tag{2}$$

where R_{φ} represents a rotation matrix of angle φ and $M_{\lambda/m}$ is the Jones matrix of a λ/m plate. $\Delta\phi = \phi_0 + \phi_E$ is the sum of the two contributions to the phase difference between the two eigenpolarizations in the EO crystal. ϕ_0 is linked to its intrinsic birefringence which is temperature dependent. The Jones' matrix of the PMF writes:

$$M_{PMF} = \begin{pmatrix} \exp(-j\theta/2) & 0 \\ 0 & \exp(j\theta/2) \end{pmatrix}. \tag{3}$$

Consequently, the Jones' matrix of the optical system from the entrance of the PMF up to the entrance of the 1st Wollaston prism is given by:

$$M_{system} = R_{-\varphi_{H1}} \cdot R_{\lambda/2} \cdot R_{\varphi_{H1}-\varphi_{Q1}} \cdot R_{\lambda/4} \cdot R_{\varphi_{Q1}} \cdot M_{PMF} \cdot R_{-\pi/4} \cdot M_{probe} \cdot R_{\pi/4} \cdot M_{PMF}\,. \tag{4}$$

As the input polarization state of the laser probe beam at the entrance of the system is linear, the optical powers P_1 and P_2 received by the photodectectors PD1 and PD2 write:

$$\begin{pmatrix} P_1 \\ P_2 \end{pmatrix} \equiv \left| M_{system} \cdot \begin{pmatrix} 0 \\ 1 \end{pmatrix} \right|^2 . \tag{5}$$

The calculation of these optical powers leads to:

$$\begin{aligned} P_{\substack{1\\2}} = \frac{1}{2}\Big\{ & 1 \pm \left(\cos 2\varphi_{Q1} \cos\Delta\phi + \sin\left(2\alpha+\theta\right) \sin 2\varphi_{Q1} \sin\Delta\phi\right) \cos\left(4\varphi_{H1} - 2\varphi_{Q1}\right) \\ & \pm \cos\left(2\alpha+\theta\right) \sin\Delta\phi \sin\left(4\varphi_{H1} - 2\varphi_{Q1}\right) \Big\} \end{aligned} . \tag{6}$$

As the optimal working point corresponds simultaneously to balanced optical powers in absence of applied E field ($P_1 = P_2$ for $\phi_E = 0$) and to a zero of the second derivative $\frac{\partial^2 P_{1,2}}{\partial \phi_E{}^2}$ (which is fully equivalent to the equality $P_3 = P_4$), we can therefore calculate the orientations of the two wave plates Q1 and H1:

$$\begin{aligned} \varphi_{Q1} &= \frac{1}{2} \arccos\left(\delta \frac{\sin\phi_0}{\sqrt{1-\cos^2\left(2\alpha+\theta\right)\cos^2\phi_0}} \right) \\ \varphi_{H1} &= \frac{1}{4}\left\{ 2\varphi_{Q1} + \arctan\left(-\cos\left(2\alpha+\theta\right), \frac{\cos 2\varphi_{Q1}}{\tan\phi_0} + \sin\left(2\alpha+\theta\right)\sin 2\varphi_{Q1} \right) \right\} \end{aligned} , \tag{7}$$

where $\delta = 2\left\{ \left(\left\lfloor \frac{2\alpha+\theta}{\pi} \right\rfloor + \left\lfloor \frac{\phi_0 - 3\pi/2}{\pi} \right\rfloor \right) \bmod 2 - \frac{1}{2} \right\}$ is equal to ± 1 ($\lfloor x \rfloor$ is the round down of x to the nearest integer). From the above-mentioned conditions required for the optimization of the system and Eq. (7) we can express ϕ_0 and θ in function of the experimental parameters φ_{Q1}, φ_{H1} and α, easily attainable by the experimenter. We get:

$$\theta = \arctan\left(\tan\left(4\varphi_{H1} - 2\varphi_{Q1}\right), \sin 2\varphi_{Q1}\right) - 2\alpha$$
$$\phi_0 = \Psi \,\mathrm{sgn}\left(\varphi_{H1} - \frac{\pi}{8} + \frac{\Psi}{4}\right) \quad \text{with} \quad \Psi = \arctan\left(\sqrt{\tan^2\left(4\varphi_{H1} - 2\varphi_{Q1}\right) + \sin^2 2\varphi_{Q1}}, \cos 2\varphi_{Q1}\right) \tag{8}$$

where $\arctan(x, y) = \arctan(y/x)$.

Let us remark that the dephasing ϕ_0 which is linked to the intrinsic birefringence of the EO crystal is fully determined by the orientation of the two wave plates Q1 and H1, regardless of EO crystal orientation α. Consequently, no specific orientation of the EO crystal is required for a simultaneous measurement of the applied E field and the temperature of the crystal.

Experimental validation

In order to get a real-time tracking of the optimal working point of the system, the two wave plates H1 and Q1 (see Fig. 1) have been mounted on motorized rotation stages, the orientation of these two wave plates being controlled by PID regulation loops that use the currents of the four photodiodes PD1 to PD4 as inputs. With such a servo-controlled system, we get at any time $P_1 = P_2$ and $P_3 = P_4$, ensuring a constant response of the measure with both highest linearity and sensitivity as shown in the previous section. Fig. 3 shows a single shot vertically polarized HPM signal emitted by a horn antenna and measured simultaneously by the EO probe and a reference antenna. The reference antenna and the EO probe were located at a distance of 5 m and 2 m from the emitting horn, respectively, both detectors being in the far field region. The peak amplitude of the E field radiated by the horn antenna at the EO probe location is ~ 800 kV/m while it is ~ 150 kV/m at the antenna location. For the measurement, the sensitivity axis of the EO probe, defined by the direction of the sensitivity vector $\overrightarrow{\Delta K}$, has been vertically aligned. Another measurement is presented in Fig. 3 for which the EO probe is rotated

of 90° about its initial position getting its sensitivity axis horizontally aligned. The EO measurements have been performed using a u^2t high speed 45-GHz bandwidth photodiode as PD1 followed by a Miteq 22-dB gain 0.1-10 GHz microwave amplifier and a Tektronix 12-GHz real-time oscilloscope. As seen on Fig. 3, the reference antenna and the EO probe deliver a very similar signal. Moreover, the signal vanishes when the EO probe has been rotated of 90°. However, only qualitative comparisons can be made in the time-domain. In order to get a more quantitative comparison, the spectra have been calculated by fast Fourier transform: They are plotted in Fig. 4. We can see that nearly identical spectra are obtained with the reference antenna (dotted line) and the EO probe (solid line). Moreover, an extinction of ~ 20 dB is observed when the EO probe has been rotated, confirming the ability of such sensor to measure a unique E-field component. For that purpose, the EO crystal has been processed in a cylindrical shape in order to keep the same orientation of the ambient E field to be measured and the inner-EO crystal E field that is actually measured [18]. For reference antenna and EO probe, the noise level comparison of the spectra of measured signals on one hand and of the incident E-field level on the other hand, leads to an estimation of a ~30 dB loss of signal-to-noise ratio when the reference antenna is substituted by the EO probe. Nevertheless, it is the only drawback when comparing the relative performances of the reference antenna and the EO probe as the EO probe presents a millimetrical spatial resolution, a flat frequency response from quasi DC up to a few tens of GHz and almost no invasiveness due to its fully dielectric making.

In the theoretical section, we have shown that the dephasings ϕ_0 and θ, linked to the intrinsic birefringence of the EO crystal and of the PMF, respectively, can be separately determined from the orientation of the two servo-controlled wave plates. As the dephasing ϕ_0 is

essentially depending on the temperature of the EO crystal, any change of its temperature should be easily determined. In order to experimentally validate the measurement of the relative temperature of the EO probe, we have first characterized the temperature dependence of the EO crystal birefringence. For that purpose, we have used a common "polarizer – EO crystal – crossed polarizer" configuration in which the eigen dielectric axes of the EO crystal make an angle of ~45° about the polarizer axis. The transmitted optical power is modulated by the dephasing ϕ_0 and the modulation period is given by $\Delta\phi_0 = 2\pi$. Using a congruent $LiTaO_3$ crystal of length $L_{crystal} = 7.1$ mm, initially heated at 70°C, we have then recorded the transmitted optical power versus the crystal temperature *T*. From this measurement, and considering a linear variation of ϕ_0 versus *T,* we can extract the thermal dependence of the birefringence $\Delta n = n_o - n_e$ of the crystal used to build the probe:

$$\frac{\partial \Delta n}{\partial T} = \frac{\lambda}{2\pi L_{crystal}} \frac{\partial \phi_0}{\partial T}. \tag{9}$$

We have obtained a value of ~5.5 ± 0.5 10^{-5} K^{-1} much higher than in the case of stoichiometric $LiTaO_3$ crystal [19].

We have then put only the tip of the EO probe in an oven, initially heated above room temperature. During its return to the thermal equilibrium, the orientations of the two servo controlled wave plates H1 and Q1 have been recorded (see Fig. 5). We have simultaneously recorded the temperature of the oven using a K-type thermocouple (nickel-chromium) that has been put close to EO crystal. The dephasing ϕ_0, calculated using Eq. (8) from data of Fig. 5 is shown in Fig. 6 (solid line). ϕ_0 exhibits some artificial π-phase jumps from -90° to +90°

resulting from the "arctan" function appearing in Eq. (8). Once unfolded, ϕ_0 presents an exponential decreasing shape (see dotted line curve on Fig. 6). The small spikes present on the folded and unfolded curves appear each time the servo-controlled system is tracking a new working point, resulting in orientation jumps of the waveplates that appear in Fig. 5. Then, the temporal evolution of the temperature of the EO probe tip has been calculated from the value of the thermal dependence of the EO crystal birefringence that we have measured and from the unfolded ϕ_0 curve. For this calculation, we have used Eq. (9) in which $L_{crystal}$ has been replaced by twice the physical length of the EO crystal in order to take the back and forth travel of the laser probe beam inside the EO probe into account. This temporal evolution is represented in Fig. 7 together with the direct temperature measurement obtained with the thermocouple. The only adjustable parameter that has been used to calculate the temperature from the unfolded ϕ_0 curve is the initial temperature (at $t = 0$). Indeed, we have only access to the variations of ϕ_0 as its absolute value is unknown. Concerning the second fitting parameter ($\partial \Delta n / \partial T$) we have considered a value of 5.37 10^{-5} K^{-1} to get the best agreement between the two measurements. Let us notice that this value is fully consistent with the value of $\partial \Delta n / \partial T$ already measured (5.5 ± 0.5 10^{-5} K^{-1}), thus validating temperature measurements with the EO probe. Moreover, we get a much lower *rms* noise on the temperature curve obtained with the EO probe than the one obtained with the thermocouple, even considering phases of new working point tracking involving the spikes. In order to evaluate the temperature measurement accuracy of the EO probe, we have fitted the experimental curve with a theoretical adjustment (dotted line on Fig. 7) composed of an exponential decay term and a linear term. This latter term (3 mK s^{-1} decay) has been added to the natural exponential decay term (time constant $R_{oven}C_{oven}$ of 0.6 ks) in order to

take the slow drift of the ambient temperature into account. Since the time constant $R_{oven}C_{oven}$ is much larger than the one of the EO crystal, the temperature given by the thermocouple on one hand, and the EO crystal on the other hand, should be the same. As seen, the experimental temperature measured with the EO probe is almost indiscernible from the theoretical fit. To the first order, we can estimate that the temperature accuracy of our EO probe is given by the standard deviation between the theoretical fit and the experimental data: a value of 55 mK is obtained. When the spikes (representing ~1% of the data) are excluded, this value is reduced to 40 mK! Indeed, the EO probe is not only a fully dielectric, non invasive and miniature electric field sensor (see photo in Fig. 2) but constitutes also a very precise temperature sensor.

Conclusion

We have developed new miniature, non invasive and fully dielectric EO probes that present an ultra wide bandwidth. Although presenting a lower sensitivity compared to antenna, such probes have a flat response from 1 kHz to a few tens of GHz and a large dynamic of measurement making them perfectly suited for high power microwave measurements. Up to now, all EO probes that were based on polarization state modulation were suffering of their huge sensitivity to the temperature that forbids their use outside thermally regulated laboratories. With the new design of EO probe proposed in this paper, we have turned this major drawback into advantage as our EO probes are able to measure temperature with a relative accuracy of the order of 40 mK. Moreover, the servo-controlled system is able to maintain an optimal working point for hours with temperature variations of the EO probe as fast as 0,02 °C per second. Finally, the authors would like to acknowledge the DGA (French Military Programs Management and Procurement Agency) for their support.

References

1. W. D. Parther, C. E. Baum, R. J. Torres, F. Sabath, and D. Nitsch, "Survey of worldwide high-power wideband capabilities," IEEE Trans. Electromagn. Compat. **46**, 335-344 (2004).
2. S. Wakana, T. Ohara, M. Abe, E. Yamazaki, M. Kishi, and M. Tsuchiya, "Fiber-edge electrooptic/magnetooptic probe for spectral-domain analysis of electromagnetic field", IEEE Trans. Microwave Theory Tech. **48**, 2611-2616 (2000).
3. G. Zheng, J. Xu, L. Chen, H. Wang, and W. She, "Athermal design for the potassium titanyl phosphate electro-optical modulator," Appl. Opt. **46**, 6774-6778 (2007).
4. R. Forber, W.C. Wang, D.-Y. Zang, S. Schultz, and R. Selfridge, "Dielectric EM field probes for HPM test & evaluation," presented at the Annual ITEA Technology Review, Cambridge, United Kingdom, 7-10 August 2007.
5. M.-S. Huang, M.-H. Lu, and J.-T. Shy, "High sensitivity bulk electro-optic modulator field sensor for high voltage environments", *Rev. Sci. Instrum.* **75**, 5364-5366 (2004).
6. V. N. Filippov, A. N. Starodumov, Y. O. Barmenkov, and V. V. Makarov, "Fiber-optic voltage sensor based on a $Bi_{12}TiO_{20}$ crystal", *Appl. Opt.* **9**, 1389-1393 (2000).
7. R. Claverie, J.-P. Salvestrini, and M. D. Fontana, "New electro-optic sensor architecture for temperature measurements," presented at the Instrumentation and Measurement Technology Conference, Varsaw, Poland, 1-3 May 2007.
8. B. Mellouet, L. Velasco, and J. Achkar, "Fast method applied to the measurement of microwave power standards," IEEE Trans. Instrum. Meas. **50**, 381-384 (2001).
9. G. C. Baldwin, An Introduction to Non Linear Optics (Plenum Press, 1969).
10. B. H. Kolner and D. M. Bloom, "Electro-optic sampling in GaAs integrated circuits," IEEE J. Quantum Electron. **22,** 79–93 (1986).

11. K. Yang, L. P. B. Katehi, and J. F. Whitaker, "Electro-optic field mapping system utilizing external gallium arsenide probes," Appl. Phys. Lett. **77**, 486-488 (2000).
12. L. Levi, Applied Optics Vol. 2, (Wiley & Sons, 1980).
13. R. B. Dyott, Elliptical Fiber Waveguides, (Artech House, 1995).
14. L. Duvillaret, S. Rialland, and J.-L. Coutaz, "Electro-optic sensors for electric-field measurements. I. Theoretical comparison among different modulation techniques," J. Opt. Soc. Am. B **19,** 2692–2703 (2002).
15. L. Duvillaret, S. Rialland, and J.-L. Coutaz, "Electro-optic sensors for electric-field measurements. II. Choice of the crystals and complete optimization of their orientation," J. Opt. Soc. Am. B **19,** 2704–2715 (2002).
16. B. E. A. Saleh and M. C. Teich, Fundamentals of Photonics, (Wiley-Interscience, 1991).
17. L. Duvillaret and G. Gaborit, "Sonde électro-optique de mesure de température et de champ électromagnétique," French patent deposit 06-52156 (2006).
18. G. Gaborit, J.-L. Coutaz, and L. Duvillaret, "Vectorial electric field measurement using isotropic electro-optic crystals," Appl. Phys. Lett. **90**, 241118 (2007).
19. K. S. Abedin and H. Ito, "Temperature-dependent dispersion relation of ferroelectric lithium tantalate," J. Appl. Phys. **80**, 6561-6563 (1996).

Figure Captions

Fig. 1. Experimental setup (PD = photodiode, LD = laser diode, BS = non polarizing beam splitter, EO = electro-optic).

Fig. 2. Schematic and picture of the EO probe with indication of the relative orientations of the eigen dielectric axes of the probe optical elements.

Fig. 3. Single shot vertically polarized high power microwave signal measurement obtained with (a) a reference antenna (b) the EO probe having its sensitivity vector $\overrightarrow{\Delta K}$ vertically aligned (c) the EO probe having its sensitivity vector $\overrightarrow{\Delta K}$ horizontally aligned (an artificial offset has been added for clarity).

Fig. 4. Spectra of the single shot high power microwave signal (see Fig. 3) measured with a reference antenna (dotted line), the EO probe having its sensitivity vector $\overrightarrow{\Delta K}$ vertically aligned (solid line), and the EO probe having its sensitivity vector $\overrightarrow{\Delta K}$ horizontally aligned (dots).

Fig. 5. Temporal record of the orientations of the two servo-controlled wave plates Q1 and H1 used to lock the optical system on an optimal working point during the cool down of the EO probe.

Fig. 6. Folded (solid line) and unfolded (dotted line) dephasing ϕ_0 introduced between the two eigen polarization states inside the EO crystal during its cool down and calculated from the wave plates orientations given in Fig. 5.

Fig. 7. Temperature of the EO probe calculated from the dephasing ϕ_0 plotted in Fig. 6 (solid line) and simultaneously measured with a thermocouple (crosses). A theoretical adjustment of the EO probe temperature is also represented in dotted line.

Fig. 1

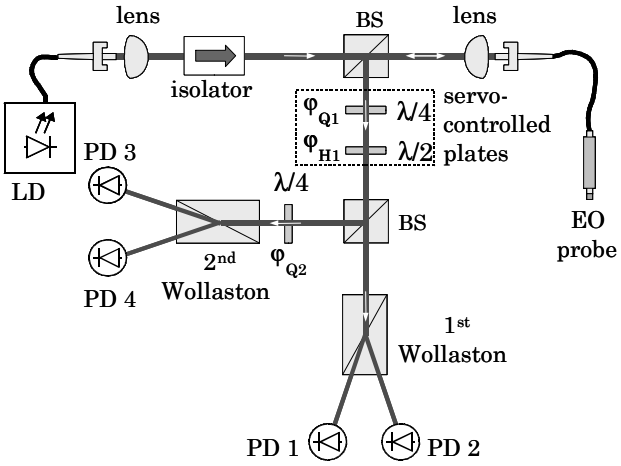
lens
BS
lens
isolator
φ_{Q1}
λ/4
φ_{H1}
λ/2
servo-
controlled
plates
PD 3
LD
λ/4
BS
EO
probe
2nd
Wollaston
φ_{Q2}
PD 4
1st
Wollaston
PD 1
PD 2

Fig. 2

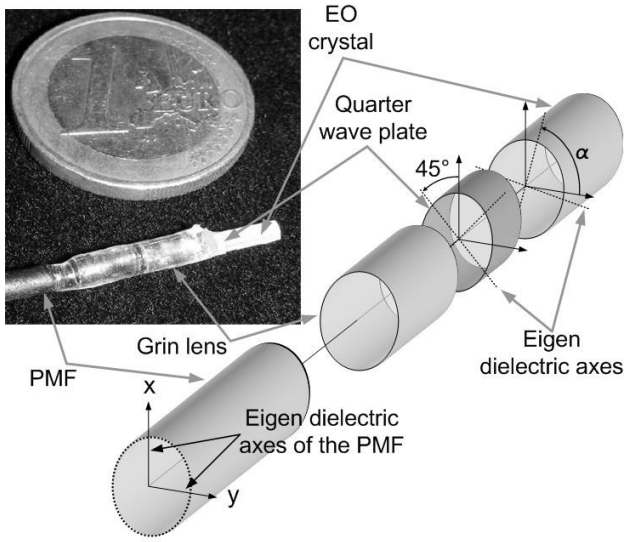
EO
crystal
Quarter
wave plate
45°
α
Grin lens
PMF
x
Eigen dielectric
axes of the PMF
y
Eigen
dielectric axes

Fig. 3

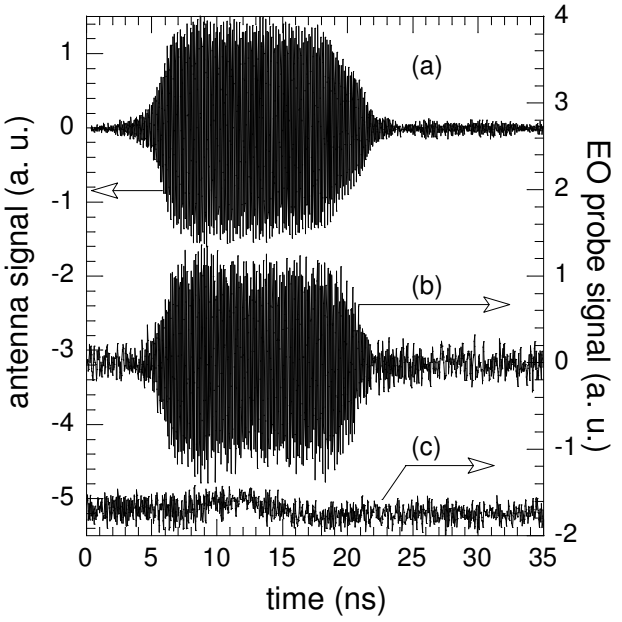
antenna signal (a. u.)
EO probe signal (a. u.)
time (ns)
(a)
(b)
(c)
1
0
-1
-2
-3
-4
-5
4
3
2
1
0
-1
-2
0
5
10
15
20
25
30
35

Fig. 4

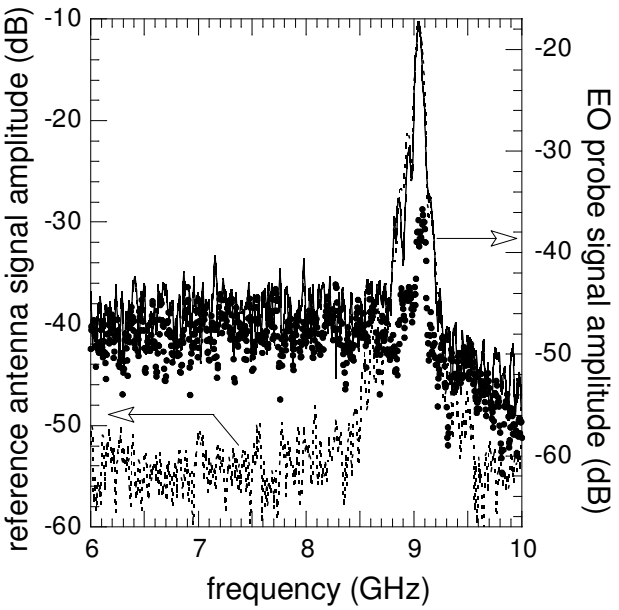
reference antenna signal amplitude (dB)
EO probe signal amplitude (dB)
frequency (GHz)
-10
-20
-30
-40
-50
-60
6
7
8
9
10

Fig. 5

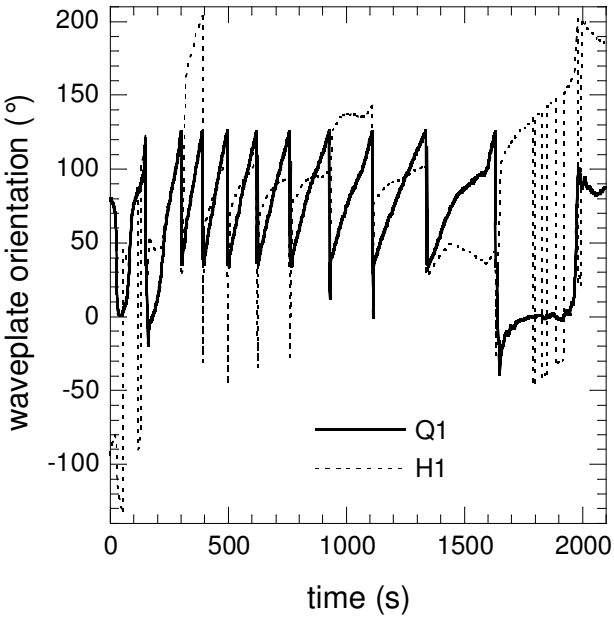
waveplate orientation (°)
200
150
100
50
0
-50
-100
0
500
1000
1500
2000
time (s)
Q1
H1

Fig. 6

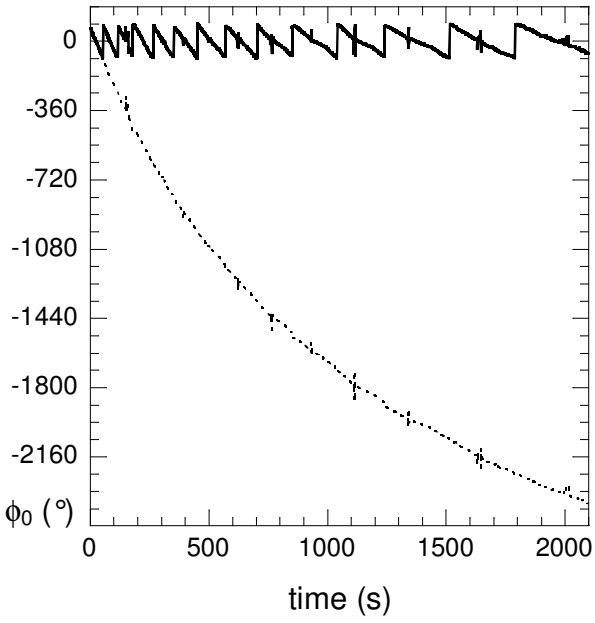

Fig. 7

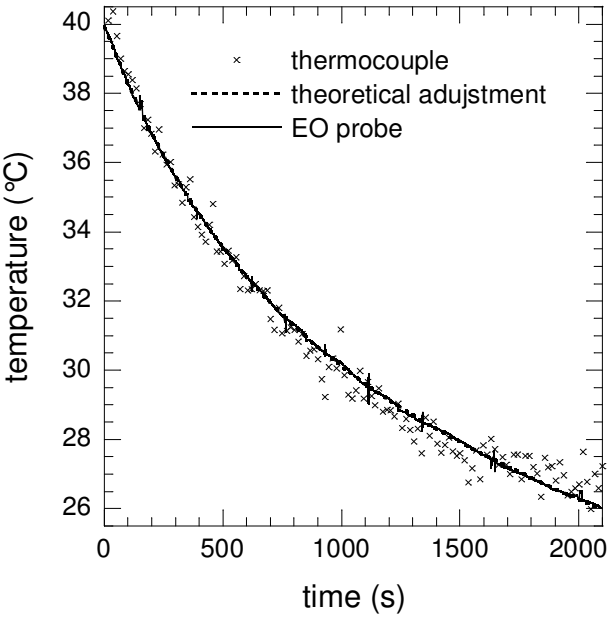
thermocouple
theoretical adujstment
EO probe
temperature (°C)
time (s)
40
38
36
34
32
30
28
26
0
500
1000
1500
2000